

Supporting Information

Arm Growth and Facet Modulation in Perovskite Nanocrystals

Lucheng Peng,^{¥,1} Sumit Kumar Dutta,^{¥,2} Debayan Mondal,³ Biswajit Hudait,² Sanjib Shyamal,² Renguo Xie,^{1,*} Priya Mahadevan^{3,*} Narayan Pradhan^{2,*}

¹State Key Laboratory of Inorganic Synthesis and Preparative Chemistry, College of Chemistry Jilin University, Changchun 130012, China

²School of Materials Sciences, Indian Association for the Cultivation of Science, Kolkata, 700032 India

³Department of Condensed Matter Physics and Material Science, S. N. Bose National Centre for Basic Sciences, Kolkata 700106 India

[¥]Both authors have equal contributions

Emails: (NP) camnp@iacs.res.in

Details of DFT calculations:

The Surface energies of CsPbBr₃ were calculated using a projected augmented wave (PAW)^{1, 2} implementation of density functional theory within the Vienna ab initio simulation package (VASP).^{3, 4} The generalized gradient approximation (GGA)⁵ was used for the exchange-correlation functional. The DFT-D2 method of Grimme⁶ was considered to introduce dispersive interactions within the system. A gamma-centered Monkhorst-Pack k mesh of 4 × 4 × 2 was used to perform the k-space integrations. In addition to this, an energy cut-off of 400 eV was used for the kinetic energy of the plane waves included in the basis. At room temperature, bulk CsPbBr₃ exhibits an orthorhombic structure with space group symmetry Pbnm. The experimental lattice parameters⁷ which are a = 8.21 Å; b = 8.28 Å and c = 11.80 Å were used in the calculations. To ensure the convergence of the results with respect to the slab size, slab sizes of 9 and 17 number of layers were considered in the calculations. The results for the larger slab size have been reported in this manuscript, though the results from the smaller slab are qualitatively similar. To explore the influence of different experimental conditions on the growth, symmetric slabs have been constructed for each of the surfaces considered. The terminating layer in each facet considered have been indicated in Table S3. Most of the earlier work in the literature has been carried out for {110} surfaces. Here, it has been shown that the CsBr terminated surface is more favourable⁸, and so the calculations have been performed for CsBr terminated surfaces. The implementation of density functional theory that is used in this work requires periodicity of the lattice. Hence, consecutive slabs separated by a vacuum of 20 Å have been used in the calculations to ensure that the periodically repeated units in the growth direction are well decoupled. As there are dangling bonds states associated with the surface layer for {100}, {012} and {112} surfaces, the surface Pb atoms in these cases have been passivated with pseudo-hydrogens. For each of the surfaces considered, while the lattice constants were fixed at the experimental values, the internal positions were allowed to vary so as to minimize the total energy. The optimized structures in each case were used to calculate the surface energy. The surface energy⁹ is given by eq. 1 below where μ_{Cs} , μ_{Pb} , and μ_{Br} are the chemical potentials for Cs, Pb and Br respectively.

$$\Omega = \frac{1}{2} [E_{CsPbBr_3}^{Slab} - N_{Cs}\mu_{Cs} - N_{Pb}\mu_{Pb} - N_{Br}\mu_{Br}] \quad (1)$$

Here $E_{CsPbBr_3}^{Slab}$ refers to the total energy of the slab, N_{Cs} , N_{Pb} , and N_{Br} are the number of Cs cations, Pb and Br atoms in the slab, respectively. The factor of 1/2 takes into account the existence of the two identical surfaces in the slab. The chemical potential μ_{CsPbBr_3} of a stoichiometric $CsPbBr_3$ phase is given by the sum of the three terms, representing the chemical potentials of each atomic constituent, within the crystal, as follows

$$\mu_{CsPbBr_3} = \mu_{Cs} + \mu_{Pb} + 3\mu_{Br} \quad (2)$$

As the surface is in equilibrium with the bulk $CsPbBr_3$ so we can say $\mu_{CsPbBr_3} = E_{CsPbBr_3}^{Bulk}$ using this we can rewrite the equation (1) as

$$\Omega = \frac{1}{2} [E_{CsPbBr_3}^{Slab} - N_{Cs}E_{CsPbBr_3}^{Bulk} - (N_{Pb} - N_{Cs})\mu_{Pb} - (N_{Br} - 3N_{Cs})\mu_{Br}] \quad (3)$$

In our calculation the constrained value for chemical potential of Pb and Br must satisfy the thermodynamical equilibrium growth condition for bulk $CsPbBr_3$ and also avoid the formation of CsBr as secondary phases. This places a constraint on the chemical potentials, given by

$$\Delta\mu_{Cs} + \Delta\mu_{Pb} + 3\Delta\mu_{Br} = \Delta H_{CsPbBr_3} \quad (4)$$

$$\Delta\mu_{Cs} + \Delta\mu_{Br} \leq \Delta H_{CsBr} \quad (5)$$

Here $\Delta\mu$ represents the variation of chemical potentials from the chemical potential of that element which is taken as the energy of the ground state configuration of that particular element. We have taken the most stable crystal structure for Pb^{10} and Cs^{11} . For Br we consider Br_2 dimer in a large cubic unit cell of dimension 10 Å. A similar calculation was performed for H_2 as well as CH_3NH_3 ion. ΔH_{AB} is the formation energy of the compound AB^{12} . The formation energy of $CsPbBr_3$ (ΔH_{CsPbBr_3}) and $CsBr$ (ΔH_{CsBr}) were calculated to be -9.838 eV and -2.377 eV respectively.

The surface energy given by Table S3 is calculated for different facets under the Br poor condition where $\Delta\mu_{Cs} = 0.0$, $\Delta\mu_{Pb} = -2.72$ eV, $\Delta\mu_{Br} = -2.370$ eV and $\Delta\mu_H = 0$ eV. This condition satisfies the requirement of Equation (4) and Equation (5). Under these condition $PbBr_2$ will be present as an impurity.

The MA ion has been seen to replace the Cs atom in earlier studies on Cs based perovskites¹³. In order to examine the conditions when the MA ion would bind to the surface Br atom, the formation energies for both cases were calculated and are given in Table S4.

Indeed under Cs poor conditions, one could have both MA ion adsorption on the surface as well as Cs atom at the surface being replaced by MA, however under moderate Cs chemical potentials or Cs rich and Bromine rich conditions one has the adsorption of the MA ion being favored. Here a modest value of $\Delta\mu_H = -1$ eV was used under Br-rich conditions to represent the allowed chemical potential variations.

The surface energy given by Table S3 were calculated for different facets under the Br rich condition where $\Delta\mu_{Cs} = -1.5$ eV, $\Delta\mu_{Pb} = -8.338$ eV, $\Delta\mu_{Br} = 0.0$ eV and $\Delta\mu_H = -1.0$ eV. This condition satisfies the requirement of Equation (4) and Equation (5). Under these condition $PbBr_2$ will be present as an impurity.

Supporting Figures

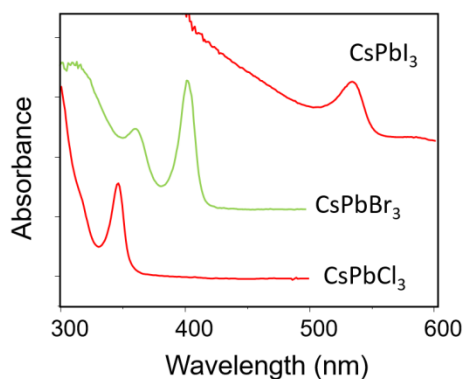


Figure S1. Absorption spectra for the seed clusters of CsPbBr₃, CsPbCl₃ and CsPbI₃. These were synthesized following our reported method¹⁴ with modification to Kovalenko and co-workers¹⁵ as mentioned in main text; but Cs(I) precursor was injected at lower (25-35 °C) temperature.

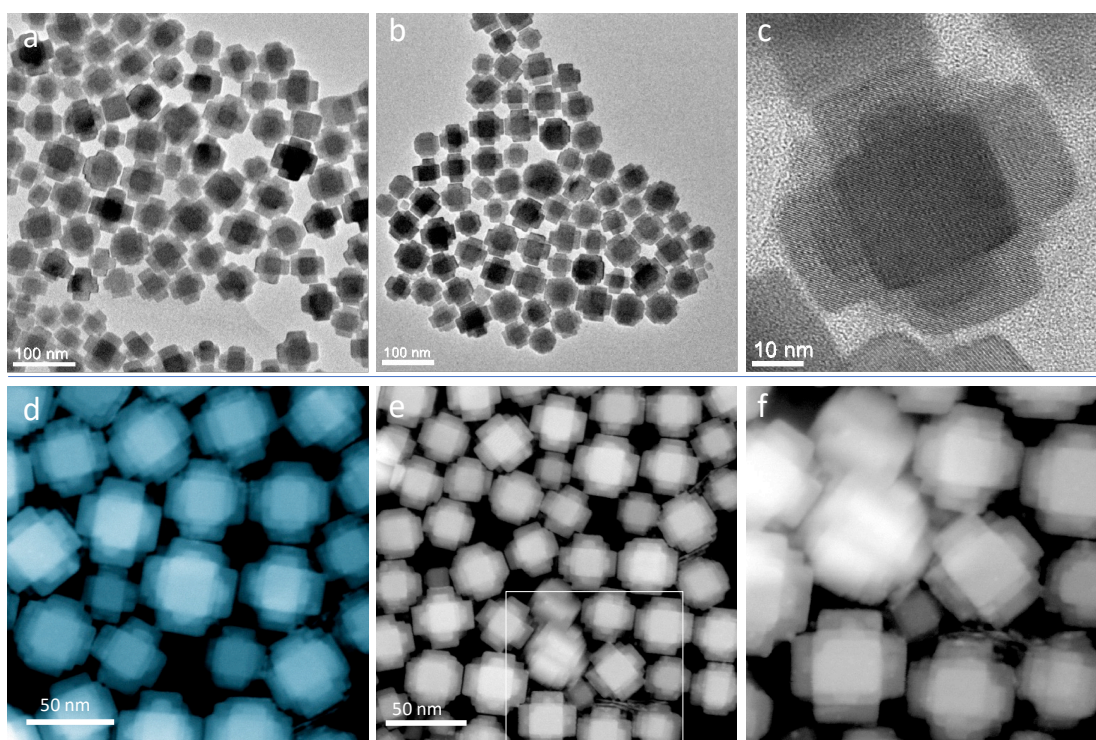


Figure S2. (a-b) TEM images and (c) HRTEM image of layered arm hexapod structures of CsPbBr₃ nanocrystals obtained from 250 °C – 280 °C reaction. Here, polyhedrons were prepared at 250 °C, OLA-HBr was injected at 250 °C and annealing was done for 5 min at 280 °C. (d-e) HAADF-STEM images of the same sample and (f) magnified image from a small area

of image (e).

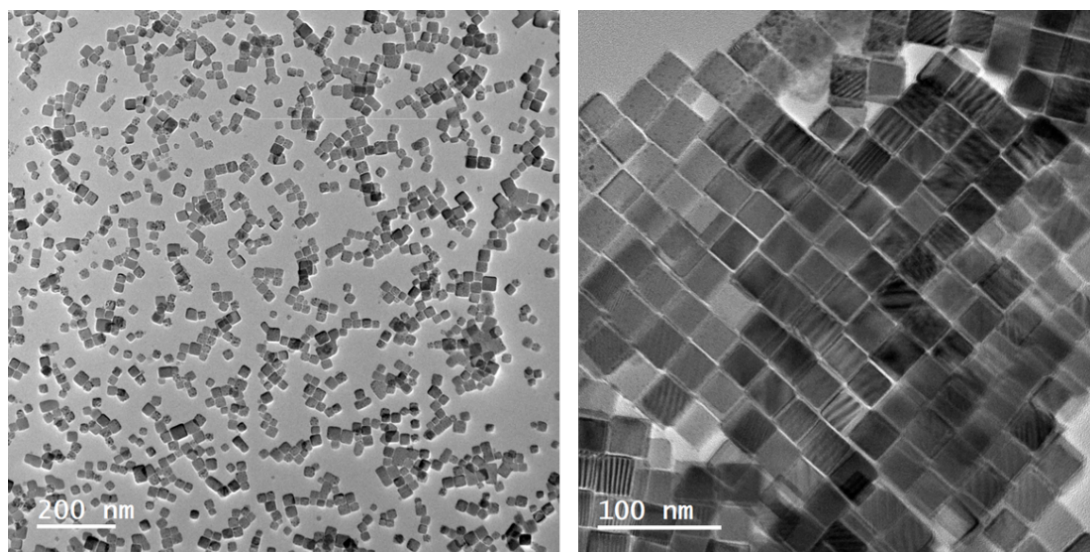


Figure S3. TEM images of CsPbBr₃ nanocubes obtained at 180 °C seed injection reactions. The images were obtained from the sample after introduction of OLA-HBr.

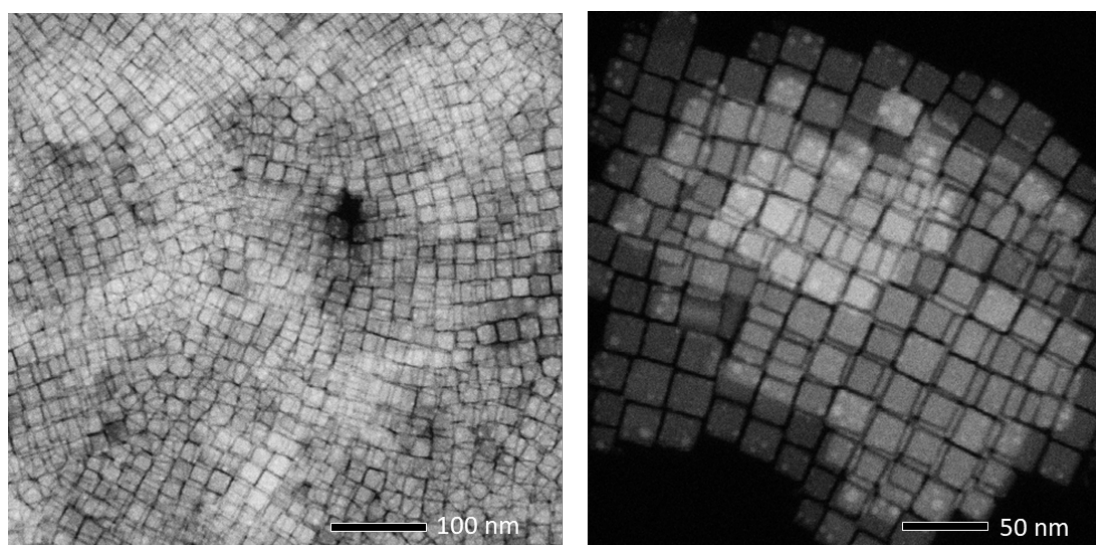


Figure S4. HAADF-STEM images of CsPbCl₃ nanocrystals obtained from 250 °C injection reactions after introduction of OLA-HCl.

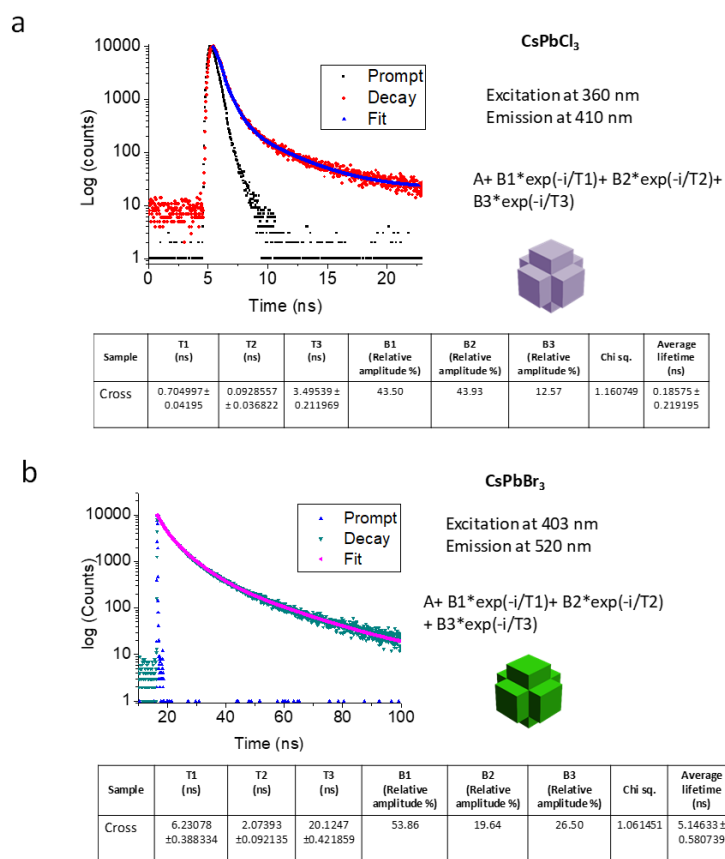


Figure S5. Excited state decay lifetime plots of (a) CsPbCl₃ and (b) CsPbBr₃ hexapod nanostructures.

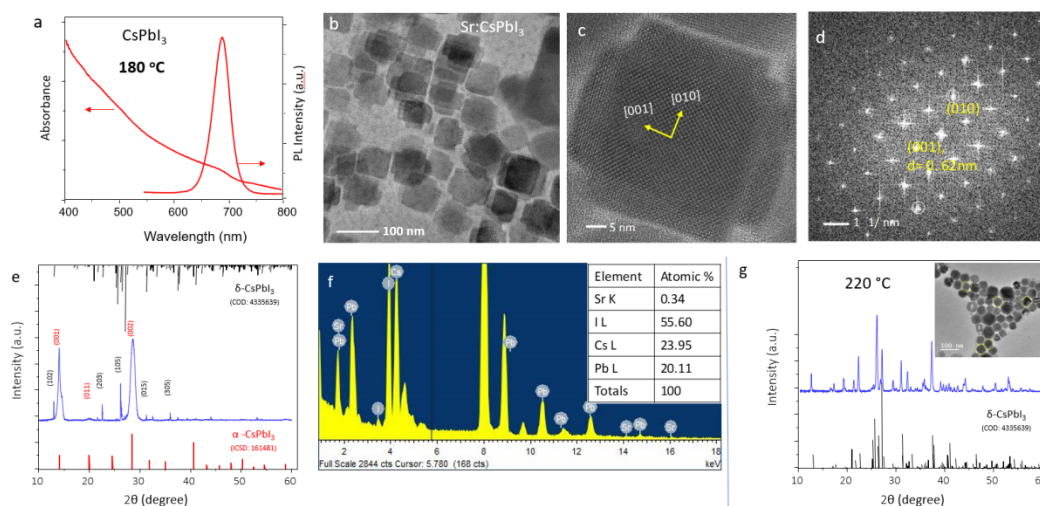


Figure S6. (a) Absorption and PL spectra of Sr(II) doped CsPbI₃ hexapods. (b) TEM, (c) HRTEM and (d) FFT pattern of these nanostructures. (e) Powder X-ray diffraction pattern of the

hexapod nanostructures which showed the mixture of phases though dominated with α -CsPbI₃. (f) EDS spectra and atomic percentage of elements. (g) Powder XRD pattern of the samples obtained from the reaction carried out at 220 °C. Insert shows the corresponding TEM image dominated with hexagonal shaped δ -CsPbI₃ nanostructures.

Method: The synthesis method was followed same as for CsPbBr₃ and CsPbCl₃. Sr(II) carbonate with 1:1 molar ratio with Pb (Sr:Pb = 1:1) was taken at the beginning and at 180 °C, OLA-HI was injected. EDS showed less than 1% Sr in the sample.

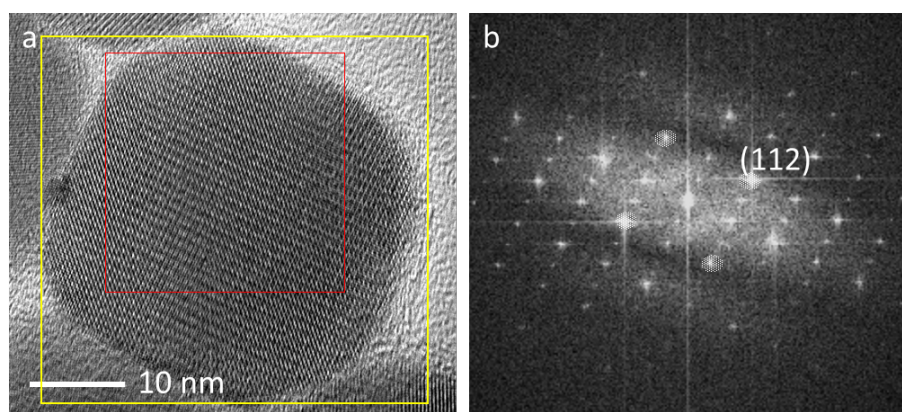


Figure S7. (a) HRTEM image of a polyhedron obtained at 230 °C, (b) selected area FFT pattern showing additional (112) planes with viewing axis along [1-10].

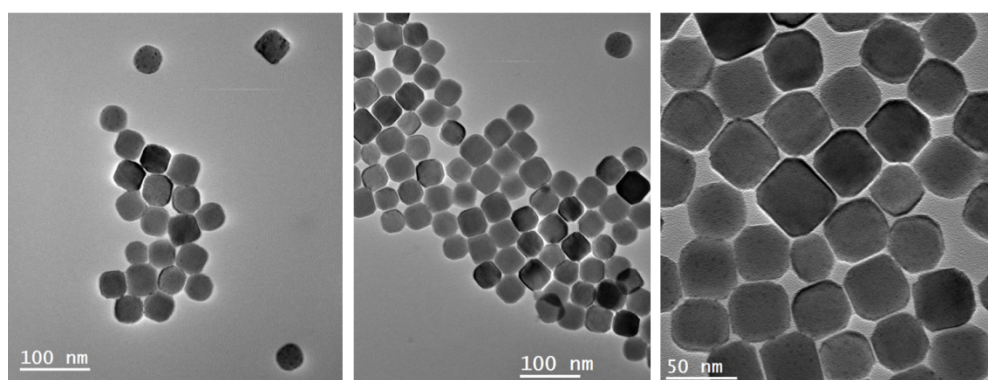


Figure S8. TEM image CsPbBr₃ polyhedrons obtained of a sample carried out from 230 °C reaction without injecting OLA-HBr.

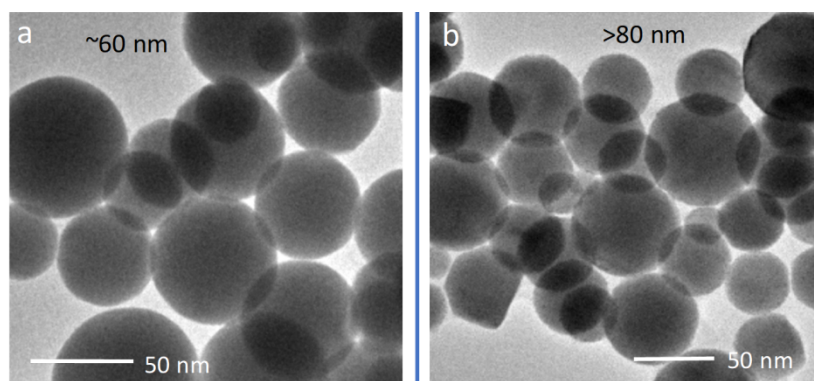


Figure S9. TEM images of (a) ~60 nm and (b) ~80 nm CsPbBr₃ polyhedron nanostructures. These nanostructures were obtained with the seed cluster injections at 250 °C with 250 °C and 280 °C annealing respectively.

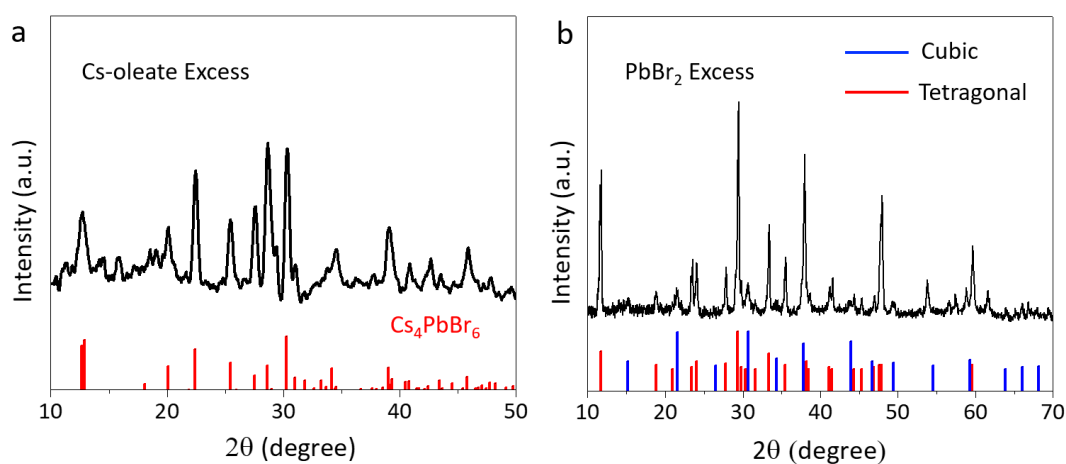


Figure S10. (a) and (b) Powder X-ray diffractions of the samples obtained from reactions with excess Cs-oleate and PbBr₂ precursors taken along with seed nanoclusters. In either case five-minute annealing at 230 °C changed the crystal phase.

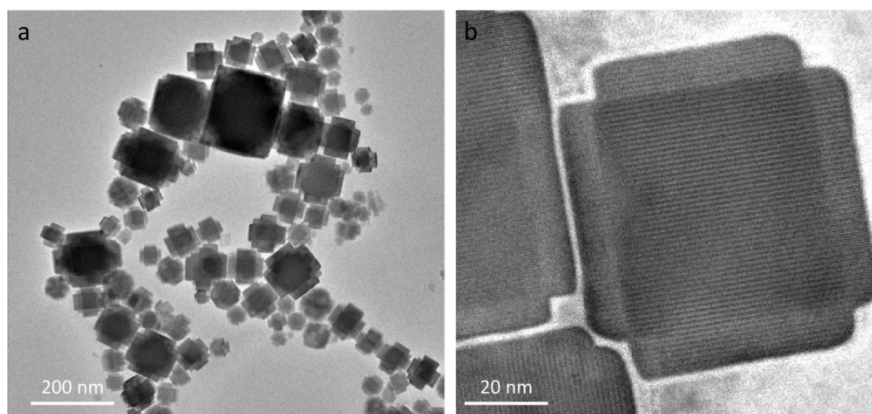


Figure S11. (a) TEM image of the hexapod nanostructures of CsPbBr₃ obtained from the reaction where TMS-Br was used as bromide source at 230 °C. (b) HRTEM image of a sample collected from a similar reaction but with ZnBr₂ treatment at 230 °C. In either case, the dispersity remained wide and could not be optimized. However, hexapods were observed in both cases. Interestingly, layered structure of hexapods arms was seen even at 230 °C reaction for TMS-Br which were typically observed at 280 °C for OLA-HBr. Reaction procedure was similar to that in case of OLA-HBr, only 0.01 ml of TMS-Br or 0.1 ml ZnBr₂ solution (0.1 mmol of anhydrous ZnBr₂ was dispersed in 1 ml ODE by sonication) was injected after 10 mins of polyhedron formation at 230 °C and annealed at that temperature for another 5 mins.

Table S1. Table of atomic percentage obtained from energy-dispersive spectroscopic (EDS) measurements carried out on polyhedron nanocrystals obtained from the reaction carried out at 230 °C reaction.

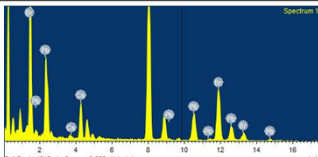
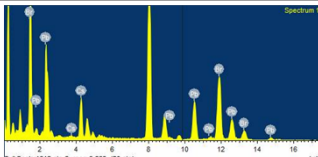
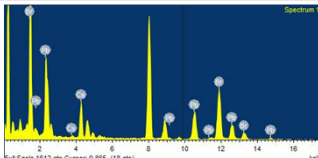
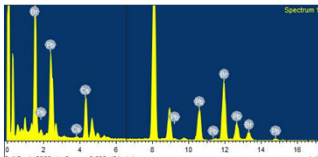
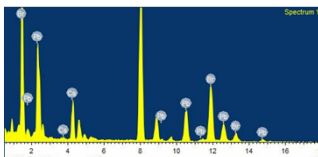
Sample	Cs (Atomic %)	Pb(Atomic %)	Br(Atomic %)	Spectra
1	20.98	23.59	55.44	
2	21.17	22.96	55.86	
3	21.45	24.97	53.58	
4	21.15	24.05	54.81	
5	23.46	25.31	51.23	

Table S2. Table of atomic percentage obtained from energy-dispersive spectroscopic (EDS) measurements carried out on hexapod nanocrystals obtained from the reaction carried out at 230 °C reaction with OLA-HBr.

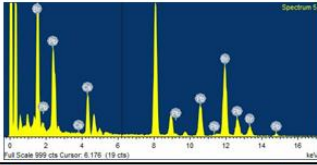
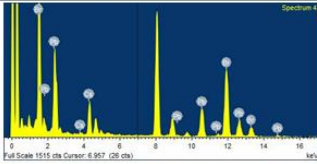
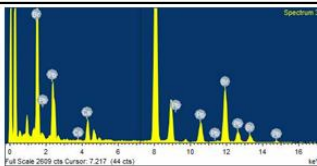
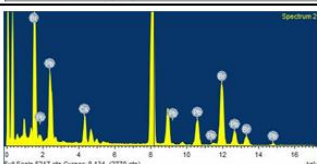
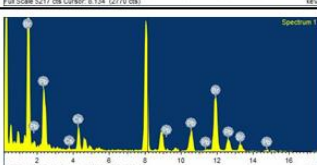
Sample	Cs (Atomic %)	Pb(Atomic %)	Br(Atomic %)	Spectra
1	18.83	21.89	59.28	
2	16.40	21.07	62.54	
3	14.71	20.17	65.12	
4	15.44	21.00	63.55	
5	15.54	23.84	66.62	

Table S3. Calculated surface energies for different facets

Facet (surface termination)	Surface Energy
(100) (CsPbBr)	$-5.229 + 2 \Delta\mu_{Br} - 4 \Delta\mu_H$
(012) (CsPbBr)	$-2.659 + 2 \Delta\mu_{Br} - 4 \Delta\mu_H$
(002) (CsBr)	$-5.204 + \Delta\mu_{Pb} + 2 \Delta\mu_{Br}$
(110) (CsBr)	$-5.159 + 2 \Delta\mu_{Pb} + 4 \Delta\mu_{Br}$
(112) (CsPbBr)	$-8.431 + 4 \Delta\mu_{Br} - 8 \Delta\mu_H$

Table S4. Calculated Formation energies for different facets for MA ion binding replacing a Cs atom and MA ion adsorbed to surface Br atom. The composition of the surface layer of each facet has been indicated.

Facet (surface termination)	Formation energy for surface Cs atom replaced by MA ion	Formation energy of MA ion adsorbed on a surface Br atom
(110) (CsBr)	$+1.982 - \Delta\mu_{CH_3NH_3} + \Delta\mu_{Cs}$	$-1.880 - \Delta\mu_{CH_3NH_3}$
(112) (CsPbBr)	$+1.980 - \Delta\mu_{CH_3NH_3} + \Delta\mu_{Cs}$	$-1.710 - \Delta\mu_{CH_3NH_3}$
(100) (CsPbBr)	$+1.334 - \Delta\mu_{CH_3NH_3} + \Delta\mu_{Cs}$	$-1.547 - \Delta\mu_{CH_3NH_3}$
(012) (CsPbBr)	$+1.703 - \Delta\mu_{CH_3NH_3} + \Delta\mu_{Cs}$	$-1.632 - \Delta\mu_{CH_3NH_3}$
(002) (CsBr)	$+0.906 - \Delta\mu_{CH_3NH_3} + \Delta\mu_{Cs}$	$-0.883 - \Delta\mu_{CH_3NH_3}$

Table S5. Formation energies calculated with the MA ion adsorbed on top of a surface Br atom and Cs is replaced by the molecule under the condition ($\Delta\mu_{Cs} = -1.5$ eV, $\Delta\mu_{Pb} = -8.338$ eV, $\Delta\mu_{Br} = 0.0$ eV and $\Delta\mu_H = -1.0$ eV).

Facet	Cs is Replaced by the molecule	Molecule is adsorbed
[110]	+0.482	-3.380
[112]	+0.480	-3.21
[100]	-0.166	-3.047
[012]	+0.203	-3.132
[002]	-0.594	-2.38

References

1. Blöchl, P. E. Projector Augmented-Wave Method. *Phys. Rev. B* **1994**, *50*, 17953-17979.
2. Kresse, G.; Joubert, D. From Ultrasoft Pseudopotentials to the Projector Augmented-Wave Method. *Phys. Rev. B* **1999**, *59*, 1758-1775.
3. Kresse, G.; Furthmüller, J. Efficient Iterative Schemes for Ab Initio Total-Energy Calculations Using a Plane-Wave Basis Set. *Phys. Rev. B* **1996**, *54*, 11169-11186.
4. Kresse, G.; Hafner, J. Ab Initio Molecular Dynamics of Liquid Metals. *Phys. Rev. B* **1993**, *47*, 558-61.
5. Perdew, J. P.; Burke, K.; Ernzerhof, M. Generalized Gradient Approximation Made Simple. *Phys. Rev. Lett.* **1996**, *77*, 3865-3868.
6. Grimme, S. Semiempirical GGA-type Density Functional Constructed with a Long-Range Dispersion Correction. *J. Comput. Chem.* **2006**, *27*, 1787-1799.
7. Bertolotti, F.; Protesescu, L.; Kovalenko, M. V.; Yakunin, S.; Cervellino, A.; Billinge, S. J. L.; Terban, M. W.; Pedersen, J. S.; Masciocchi, N.; Guagliardi, A. Coherent Nanotwins and Dynamic Disorder in Cesium Lead Halide Perovskite Nanocrystals. *ACS Nano* **2017**, *1*, 3819-3831.

8. Yang, Y.; Gao, F.; Gao, S.; Wei, S. H. Origin of the Stability of Two-Dimensional Perovskites: A First-Principles Study. *J. Mater. Chem. A* **2018**, *6*, 14949-14955.
9. Huang, X.; Paudel, T. R.; Dowben, P. A.; Dong, S.; Tsybal, E. Y. Electronic Structure and Stability of the CH₃NH₃PbBr₃ (001) Surface. *Phys. Rev. B* **2016**, *94*, 195309-195316.
10. Weir, C. E.; Piermarini, G. J.; Block, S. Crystal Structures of Cesium II and Gallium II. *J. Chem. Phys.* **1971**, *54*, 2768-2770.
11. Bouad, N.; Chapon, L.; Marin-Ayral, R. M.; Bouree-Vigneron, F.; Tedenac, J. C. Neutron Powder Diffraction Study of Strain and Crystallite Size in Mechanically Alloyed PbTe. *J. Solid State Chem.* **2003**, *173*, 189-195.
12. Mahadevan, P.; Zunger, A. Ferromagnetism in Mn-doped GaAs due to Substitutional-Interstitial Complexes. *Phys. Rev. B* **2003**, *68*, 075202.
13. Ravi, V. K.; Santra, P. K.; Joshi, N.; Chugh, J.; Singh, S. K.; Rensmo, H.; Ghosh, P.; Nag, A. Origin of the Substitution Mechanism for the Binding of Organic Ligands on the Surface of CsPbBr₃ Perovskite Nanocubes. *J. Phys. Chem. Lett.* **2017**, *8*, 4988-4994.
14. Peng, L.; Dutta, A.; Xie, R.; Yang, W.; Pradhan, N. Dot–Wire–Platelet–Cube: Step Growth and Structural Transformations in CsPbBr₃ Perovskite Nanocrystals. *ACS Energy Lett.* **2018**, *3*, 2014-2020.
15. Protesescu, L.; Yakunin, S.; Bodnarchuk, M. I.; Krieg, F.; Caputo, R.; Hendon, C. H.; Yang, R. X.; Walsh, A.; Kovalenko, M. V. Nanocrystals of Cesium Lead Halide Perovskites (CsPbX₃, X = Cl, Br, and I): Novel Optoelectronic Materials Showing Bright Emission with Wide Color Gamut. *Nano Lett.* **2015**, *15*, 3692-3696.